

Non-Compact QED₃ with $N_f \geq 2$

S.J. Hands^a, J.B. Kogut^b and C.G. Strouthos^a

^a *Department of Physics, University of Wales Swansea,
Singleton Park, Swansea, SA2 8PP, U.K.*

^b *Department of Physics, University of Illinois at Urbana-Champaign,
Urbana, Illinois 61801-3080, U.S.A.*

Abstract

Non-compact three-dimensional QED is studied by computer simulations to understand its chiral symmetry breaking features for $N_f \geq 2$, on lattice volumes up to 50^3 and bare masses as low as $m_0 a = 0.0000625$. We compute the chiral condensate, scalar and pseudoscalar susceptibilities, and the masses of scalar and pseudoscalar mesons. Finite volume effects and discretisation artifacts are carefully monitored. Our results reveal no decisive signal for chiral symmetry breaking for any $N_f \geq 2$. For $N_f = 2$ the dimensionless condensate can be bounded by $\beta^2 \langle \bar{\Psi} \Psi \rangle \leq 5 \times 10^{-5}$. We also present an exploratory study of the fractionally-charged Polyakov line.

1 Introduction

Over the past few years QED₃ has attracted a lot of attention, because of potential applications to models of high T_c superconductivity [1]. It is also an interesting and challenging model field theory in its own right, which is seen as an ideal laboratory to study effects such as dynamical mass generation which may be relevant to phenomena described by more complicated gauge field theories such as technicolor [2]. In three dimensions the model is super-renormalisable, because the coupling g has mass dimension $\frac{1}{2}$ and so provides the intrinsic scale of the theory independently of any bare fermion mass m_0 . This also implies asymptotic freedom, since for processes with momentum transfer $k \gg g^2$ the theory is effectively non-interacting.

Non-trivial behaviour may arise in the infra-red, however, as suggested by an expansion in $1/N_f$, where N_f is the number of (four-component) fermion species [3]. In the large- N_f limit the photon propagator is modified by the vacuum polarisation diagram from $1/k^2$ to $1/[k^2 + \frac{g^2}{8} N_f k]$; in coordinate space the logarithmic Coulomb potential is thus modified to $1/r$ for distances $r \gg (g^2 N_f)^{-1}$. Naively we deduce that the confining property of the Coulomb potential is screened by virtual $f\bar{f}$ pairs. However, consider the energy required to excite a real $f\bar{f}$ pair into the vacuum state [4]. The kinetic energy of the pair is positive and scales as r^{-1} by the uncertainty principle. For large r therefore, both kinetic and potential terms scale as r^{-1} and it becomes a delicate question which dominates. Next we note that the dimensionless interaction strength scales in this regime as N_f^{-1} , implying the possible existence of a critical N_{fc} below which the negative potential term dominates as $r \rightarrow \infty$. Since as $r \rightarrow 0$ the positive kinetic term must dominate the logarithmic Coulomb term, we deduce in this case the existence of an energy minimum at some non-zero r , implying the existence of stable $f\bar{f}$ bound states in the ground state. This semi-classical argument hence suggests a non-vanishing condensate $\langle \bar{\Psi}\Psi \rangle \neq 0$ for $N_f < N_{fc}$. Since the condensate spontaneously breaks chiral symmetry, the fermions are imbued with a dynamically-generated mass. For asymptotically large r the massive fermions decouple, ceasing to screen the charge, and the logarithmically-confining Coulomb potential is restored. The picture therefore predicts two possible phases for QED₃: for $N_f < N_{fc}$ chiral symmetry is broken, so that the only massless states are Goldstone bosons, and electric charge is logarithmically confined; for $N_f > N_{fc}$ the theory is conformal, consisting of massless fermions interacting via a long-range $1/r$ interaction.

In this paper we address the question of whether chiral symmetry is spontaneously broken in QED₃ for any value of $N_f \geq 2$, i.e. whether $\langle \bar{\Psi}\Psi \rangle \neq 0$ in the chiral limit bare fermion mass $m_0 \rightarrow 0$ and the continuum (weak coupling) limit $g \rightarrow 0$. This question has received much study over the past decade, the principal approach being self-consistent solutions to truncated Schwinger-Dyson (SD) equation for the fermion propagator. Initial studies using the photon propagator derived from the leading order large- N_f expansion suggested that the answer is positive with $N_{fc} \simeq 3.2$ [5]. Within this framework it was shown that the dynamically generated fermion mass is much less than the coupling constant, providing a natural hierarchy of mass scales. It is also possible to consider analytically continuing to a continuous number of flavors; the model in the limit $N_f \rightarrow N_{fc}$ is then supposed to undergo an infinite-order phase transition [6]. Other studies taking non-trivial vertex corrections into

account, however, predicted chiral symmetry breaking for arbitrary N_f [7]. More recent studies which treat the vertex consistently in both numerator and denominator of the SD equations have found $N_{fc} < \infty$, with a value either in agreement with the original study [8], or a slightly higher $N_{fc} \simeq 4.3$ [9]. Other analytical approaches have also been applied. A recent renormalization group analysis predicts $3 < N_{fc} < 4$ [10]. Finally there is an argument based on the inequality

$$f_{IR} \leq f_{UV}, \quad (1)$$

where f is the absolute value of the thermodynamic free energy, and can be estimated in the relevant limits simply by counting massless degrees of freedom, either fermions or Goldstones as reviewed below. For QED₃ this yields the prediction $N_{fc} \leq \frac{3}{2}$ [11].

There have also been attempts to resolve the issue via numerical simulation of non-compact lattice QED₃. The obvious advantage of a computer simulation is that one can study any N_f without any technical assumption concerning the convergence of expansion methods. Indeed, it is also possible to study the quenched ($N_f = 0$) limit, in which case a numerical study has shown that chiral symmetry appears to be broken [12], with a dimensionless condensate $\beta^2 \langle \bar{\Psi} \Psi \rangle \simeq 5 \times 10^{-3}$, where $\beta \equiv 1/g^2 a$ is the dimensionless lattice coupling constant (a being the lattice spacing). For the unquenched theory, opinions have divided on whether N_{fc} is finite and $\simeq 3$ [4, 13], or whether chiral symmetry is broken for all N_f [14]. The most recent study with $N_f = 2$ on lattices up to 16^3 found chiral symmetry breaking with $\beta^2 \langle \bar{\Psi} \Psi \rangle \simeq 3 \times 10^{-3}$ [15]. This value is extracted, however, by simultaneous extrapolation to continuum, chiral, and thermodynamic limits, which is difficult to control since even with broken chiral symmetry there remain large finite volume effects due to the presence of a massless photon in the spectrum. For this reason it is unlikely that a numerical simulation will ever completely exclude chiral symmetry breaking for $N_f > 0$, particularly if the condensate is suppressed by a typical non-perturbative factor $\exp(-CN_f)$ [7].

In this paper we will present results of simulations on lattices considerably larger (up to 50^3) and bare fermion masses considerably smaller ($m_0 a \geq 0.0000625$) than any previous study, which enables us to approach all three limits with greater control. Our goal is to place a bound on any possible chiral condensate using as few assumptions as possible on the nature of the required extrapolations. Our conclusion is that for $N_f = 2$, $\beta^2 \langle \bar{\Psi} \Psi \rangle < 5 \times 10^{-5}$, two orders of magnitude below the quenched value. For larger N_f the condensate is smaller still. Since we see no direct evidence for chiral symmetry breaking, our results are consistent with $N_{fc} < 2$, although as explained above an exponentially suppressed condensate is almost impossible to exclude. In the next section we briefly review the model, its symmetries, and the numerical methods used to simulate it. Our numerical results for the condensate appear in Section 3, in which in addition we present results for meson masses and susceptibilities, and Polyakov lines with both integer and fractional charges. All of these subsidiary quantities reveal evidence of strong finite volume effects which makes any conclusions drawn qualitative at best. Section 4 summarises our findings.

2 The Model

The continuum Lagrangian density describing QED₃ is given in Euclidean metric by

$$\mathcal{L} = \frac{1}{4}F_{\mu\nu}F_{\mu\nu} + \bar{\Psi}_i D_\mu \gamma_\mu \Psi_i + m_0 \bar{\Psi}_i \Psi_i \quad (2)$$

where $D_\mu \equiv \partial_\mu - igA_\mu$, and $F_{\mu\nu}$ is the field strength for the abelian gauge field A_μ . The fermions Ψ_i , $i = 1, \dots, N_f$, are four-component spinors acted on by hermitian Dirac matrices γ_μ , implying that the mass term proportional to m_0 is invariant under the 2+1 dimensional parity transformation.

Since the γ -matrices belong to a reducible representation of the Dirac algebra in three dimensions, the global symmetry of (2) is larger than naively expected. The matrices $\{\mathbf{1}, \gamma_3, \gamma_5, \tau_3\}$ where $\tau_3 \equiv i\gamma_3\gamma_5$ generate a global U(2) symmetry. To see this define $\tilde{\Psi} \equiv \bar{\Psi}\tau_3$. For $m_0 = 0$ the U(2) symmetry is then

$$\Psi \rightarrow U\Psi \quad \tilde{\Psi} \rightarrow \tilde{\Psi}U^\dagger \quad U \in \text{U}(2). \quad (3)$$

The symmetry is broken, either explicitly by a bare mass or spontaneously by chiral condensation $\langle \bar{\Psi}\Psi \rangle \neq 0$, to a residual $\text{U}(1) \otimes \text{U}(1)_{\tau_3}$ where the first U(1) factor corresponds to global fermion number conservation, and the second to a symmetry

$$\Psi \rightarrow e^{i\alpha\tau_3}\Psi \quad \tilde{\Psi} \rightarrow \tilde{\Psi}e^{-i\alpha\tau_3}. \quad (4)$$

Chiral symmetry breaking for the theory with N_f flavors would then result in the pattern $\text{U}(2N_f) \rightarrow \text{U}(N_f) \otimes \text{U}(N_f)_{\tau_3}$.

The lattice action using staggered lattice fermion fields $\chi, \bar{\chi}$ is given by

$$\begin{aligned} S &= \frac{\beta}{2} \sum_{x,\mu<\nu} F_{\mu\nu}(x)F_{\mu\nu}(x) + \sum_{i=1}^N \sum_{x,x'} \bar{\chi}_i(x)M(x,x')\chi_i(x') \quad (5) \\ F_{\mu\nu}(x) &\equiv \theta_{x\mu} + \theta_{x+\hat{\mu},\nu} - \theta_{x+\hat{\nu},\mu} - \theta_{x\nu} \\ M(x,x') &\equiv m_0\delta_{x,x'} + \frac{1}{2} \sum_{\mu} \eta_\mu(x) [\delta_{x',x+\hat{\mu}}U_{x\mu} - \delta_{x',x-\hat{\mu}}U_{x-\hat{\mu},\mu}^\dagger]. \end{aligned}$$

The vectors x, x' consist of three integers (x_0, x_1, x_2) labelling the sites of an L^3 lattice. Since the gauge action F^2 is unbounded from above, (5) defines the *non-compact* formulation of lattice QED₃. The $\eta_\mu(x)$ are Kawamoto-Smit phases ($\eta_1(x) = 1$; $\eta_2(x) = (-1)^{x_1}$; $\eta_0(x) = (-1)^{x_1+x_2}$) designed to ensure relativistic covariance in the continuum limit. For the fermion fields antiperiodic boundary conditions are used in the timelike direction and periodic boundary conditions in the spatial directions. The phase factors in the fermion bilinear are defined by $U_{x\mu} \equiv \exp(i\theta_{x\mu})$, where $\theta_{x\mu}$ is the gauge potential. In terms of continuum quantities, $\theta_{x\mu} = agA_\mu(x)$ and the coupling $\beta \equiv \frac{1}{g^2a}$, where a is the physical lattice spacing. We prefer the non-compact version of lattice QED₃, because it resembles more closely the continuum model we wish to compare with. In particular, magnetic monopole excitations, which are known to have a decisive effect on the infra-red behaviour of the compact model [16], are here strongly suppressed as β is made large.

The particle content of eq.(5) has been analysed in [17], showing that in the long-wavelength limit N flavors of staggered lattice fermion correspond to $N_f = 2N$ of the four-component continuum flavors described by the action (2). For lattice spacing $a > 0$, however, the global symmetries for $m_0 = 0$ are only partially realised. In this case the symmetry is

$$\begin{aligned}\bar{\chi}_o &\rightarrow \bar{\chi}_o e^{i\alpha} & \chi_e &\rightarrow e^{-i\alpha} \chi_e \\ \bar{\chi}_e &\rightarrow \bar{\chi}_e e^{i\beta} & \chi_o &\rightarrow e^{-i\beta} \chi_o,\end{aligned}\tag{6}$$

where $\chi_{o/e}$ denotes the field on odd (i.e. $\varepsilon(x) \equiv (-1)^{x_1+x_2+x_3} = -1$) and even sublattices respectively. Chiral symmetry breaking characterised by $\langle \bar{\Psi}\Psi \rangle \equiv \langle \bar{\chi}\chi \rangle \neq 0$ now has the pattern $U(N) \otimes U(N) \rightarrow U(N)$. Only in the continuum limit $\beta \rightarrow \infty$ is the full symmetry of the continuum theory expected to be restored.

In the context of the current discussion the issue of whether the full $U(2N_f)=U(4N)$ flavor symmetry is restored in the continuum limit $\beta \rightarrow \infty$ is very important. Take for instance the considerations of ref. [11] which constrain N_{fc} via the inequality (1):

$$1 + \frac{3}{4}(4N_{fc}) \leq 1 + 2N_{fc}^2.\tag{7}$$

Here the left hand side of the inequality counts the number of massless thermodynamic degrees of freedom in the UV limit, which consist of a single bose (the photon) and $4N_f$ fermi degrees of freedom, the factor $\frac{3}{4}$ coming from the Fermi-Dirac distribution in 2+1 dimensions. The right hand side counts both the photon and the $2N_f^2$ Goldstone modes expected from the breaking $U(2N_f) \rightarrow U(N_f) \otimes U(N_f)$. Eq. (7) yields the bound $N_{fc} \leq \frac{3}{2}$. If, however, chiral symmetry broke according to the staggered pattern $U(N) \otimes U(N) \rightarrow U(N)$, then the inequality becomes

$$1 + \frac{3}{4}(8N_c) \leq 1 + N_c^2,\tag{8}$$

implying $N_{fc} = 2N_c \leq 12$ [15]. An observation of broken chiral symmetry in the $\beta \rightarrow \infty$ limit in lattice QED₃ simulations with $N_f \geq 2$ therefore implies either that the arguments leading to the constraint (1) are incorrect, or that flavor symmetry restoration does not occur in this model.

The numerical results presented here were obtained by simulating the action (5) using a standard Hybrid Monte Carlo (HMC) algorithm. The form of (5) permits an even-odd partitioning, which means that a single flavor of staggered fermion can be simulated. The minimum number of continuum flavors which can be simulated with a local action is thus $N_f = 2$. We used the following methods to optimise the performance of the HMC algorithm. Firstly the effective coupling β' used during integration of the equations of motion along a microcanonical trajectory was tuned so as to maximise the acceptance rate of the Monte Carlo procedure for a fixed microcanonical time-step $d\tau$. As the lattice size was increased $d\tau$ had to be taken smaller and the optimal β' approached β . For example for the $N_f = 2$ case on a 16^3 lattice and coupling $\beta = 0.60$ the choices $d\tau = 0.025$ and $\beta' = 0.6007$ gave acceptance rate greater than 90% for all bare masses of interest. To maintain this acceptance rate on a 32^3 lattice we used $d\tau = 0.015$ and $\beta' = 0.6004$. Secondly the Monte Carlo procedure was optimised by choosing the trajectory length at random from a Poisson distribution with mean $\bar{\tau} = 1$. This method of optimisation, which guarantees ergodicity, also decreases

autocorrelation times dramatically. Statistical errors in our measurements were calculated by jackknife blocking, which accounts for autocorrelations in a raw dataset. We found the errors remained stable as the number of blocks was varied from 10 to 50.

3 Simulation Results

3.1 Chiral Symmetry Breaking

First let us make a statement of the problem we are addressing. Since a continuous symmetry is never broken spontaneously on a finite volume, we are required to work with $m_0 \neq 0$ and study the limiting behaviour as the explicit symmetry breaking is removed. Since for an asymptotically-free theory the UV behaviour is governed by the gaussian fixed point at the origin, then the continuum limit of the model lies in the limit $\beta \rightarrow \infty$, and all physical quantities should be expressible in terms of the scale set by the dimensionful coupling g . To compare simulation results taken at different couplings (lattice spacings), therefore, it is natural to work in terms of dimensionless variables such as βm_0 , L/β , or $\beta^2 \langle \bar{\Psi} \Psi \rangle$. As the continuum limit is approached, data taken at different β should collapse onto a single curve when plotted in dimensionless units. Formally, chiral symmetry in QED₃ is broken if

$$\lim_{\beta \rightarrow \infty} \lim_{\beta m_0 \rightarrow 0} \lim_{L/\beta \rightarrow \infty} \beta^2 \langle \bar{\Psi} \Psi \rangle \neq 0. \quad (9)$$

In practice taking the limits in the required order is difficult, for several reasons: *(i)* The lattice itself distorts continuum physics considerably unless the lattice spacing a can be chosen small compared to the relevant physical wavelengths in the system - as we already mentioned in the previous section a non-zero lattice spacing breaks explicitly the continuum $U(2N_f)$ symmetry of the action; *(ii)* the size of the lattice L^3 must be large not just in dimensionless units but also compared to any dynamically generated correlations in the system; and *(iii)* the chiral extrapolation $m_0 \rightarrow 0$ requires some theoretical prejudice. If the volume is large enough, m_0 lies in the linear regime of $\langle \bar{\Psi} \Psi(m_0) \rangle = \langle \bar{\Psi} \Psi(0) \rangle + m_0 \langle \bar{\Psi} \Psi(0) \rangle' + \dots$ and linear extrapolations of the data work well. However, the chiral extrapolation is based on assumptions which are not necessarily valid when $m_0 = 0$. New physics at $m_0 = 0$ may alter the situation. In our study despite the fact that in all our simulations we reached the “linear regime” we take a conservative stance by defining an upper bound for the condensate which is half its value at the smallest m_0 .

In Fig. 1 we plot the dimensionless chiral condensate $\beta^2 \langle \bar{\Psi} \Psi \rangle$ vs. the dimensionless bare mass βm_0 for $N_f = 2, 4, 8, 16$. The coupling $\beta = 0.6$ and the lattice volume is 16^3 . We generated approximately 1000 trajectories for each data point – statistical error bars are generally smaller than the size of the symbols. As N_f increases the chiral condensate decreases (for $m_0 \geq 0$) because of increased screening of the interaction by dynamical fermions. As $m_0 \rightarrow 0$ all the curves tend to pass smoothly through the origin. There is no sign of any discontinuous behaviour as N_f is altered. This motivates us to study in more detail the pattern of chiral symmetry breaking at small N_f on larger volumes near the chiral limit.

To check whether lattice data are characteristic of the continuum limit we next plot in Fig. 2 the dimensionless chiral condensate $\beta^2 \langle \bar{\Psi} \Psi \rangle$ vs. the dimensionless fermion bare mass

βm_0 for $N_f = 2$ at different values of the coupling $\beta = 0.45, 0.60, 0.75, 0.90$. In order to disentangle the lattice discretisation effects from the finite size effects we keep the volume in physical units $(L/\beta)^3$ constant. It can be easily inferred from the graph that at strong coupling ($\beta = 0.45$) discretisation effects are significant whereas for $\beta \geq 0.60$ the lattice artifacts become small since the data almost fall on the same line within the resolution of our analysis.

Having clarified the issue of the continuum limit we next investigate the thermodynamic limit, simulating with $N_f = 2$ at $\beta = 0.6$. In Fig. 3 we present our results for $\beta^2 \langle \bar{\Psi} \Psi \rangle$ vs. βm_0 on different lattice sizes: $8^3, 16^3, 24^3, 32^3$ and 48^3 . Note that the volumes and masses explored here are considerably closer to the thermodynamic and chiral limits than those of the study of [15], for which $L/\beta \leq 32$ and $\beta m_0 \geq 0.005$. We generated 300 – 800 configurations for each data point. This enables us to expose finite size effects at different values of the fermion bare mass. Finite size effects become small (but still significant) for $L \geq 24$ ($L/\beta \geq 40$), which is consistent with the quenched results of [12]; however as L increases all the lines continue to pass smoothly through the origin, suggesting that chiral symmetry remains unbroken.

As well as the chiral condensate, we have also studied mesonic correlation functions. In many cases these quantities yield useful information about the nature of the ground state model, although they are also more prone to finite volume effects than the simple order parameter. Fig. 4 shows results from $N_f = 2$, $\beta = 0.6$ on lattice size 16^3 and 32^3 for the ratio of longitudinal to transverse susceptibilities $R \equiv \chi_l / \chi_t$, where $\chi_{l,t}$ are the integrated propagators in scalar and pseudoscalar meson channels respectively:

$$\chi_l = \sum_x \langle \bar{\chi} \chi(0) \bar{\chi} \chi(x) \rangle; \quad \chi_t = \sum_x \langle \bar{\chi} \varepsilon \chi(0) \bar{\chi} \varepsilon \chi(x) \rangle. \quad (10)$$

The longitudinal susceptibility χ_l has contributions from diagrams with both connected and disconnected fermion lines; we checked that the connected contribution is dominant throughout our parameter space. These quantities are much noisier than the chiral condensate. The transverse susceptibility is most conveniently estimated via the Ward identity $\chi_t = \langle \bar{\Psi} \Psi \rangle / m_0$. In the chiral limit we expect

$$\lim_{m_0 \rightarrow 0} R = \begin{cases} 0, & \text{chiral symmetry broken;} \\ 1, & \text{chiral symmetry unbroken.} \end{cases} \quad (11)$$

As we can see from the figure, at large values of m_0 the finite size effects are small, but become significantly larger at intermediate values of m_0 . This implies that finite volume effects are not fully under control; the fact that R from both 16^3 and 32^3 lattices appears to converge to 1 as $m_0 \rightarrow 0$ decreases does not necessarily imply chiral symmetry is unbroken. It could be attributed to finite volume effects. Nonetheless, there is no indication of any range of m_0 over which dR/dm_0 is positive, required if chiral symmetry is broken. In Fig. 5 we plot R vs. m_0 for $N_f = 2, 4$. This result is compatible with the data presented in Fig. 1, i.e. that the explicit chiral symmetry breaking at nonzero m_0 , indicated by the departure of R from unity, is stronger as N_f decreases.

In Fig. 6 we present the results for the pion mass M_π vs. fermion bare mass m_0 for $N_f = 2$, $\beta = 0.6$ and lattice sizes $16^3, 32^3, 48^3$. If the model is chirally symmetric we expect

$M_\pi \propto m_0$; otherwise from conventional PCAC arguments we expect $M_\pi \propto \sqrt{m_0}$. As in the case of R , M_π suffers from very strong finite volume effects and therefore decisive conclusions cannot be drawn. In Fig.7 we plot the pion and sigma masses vs. m_0 for $N_f = 2$, $\beta = 0.6$ and lattice size 32^3 . The masses tend to become equal as $m_0 \rightarrow 0$, and show no sign of tending to zero in the chiral limit. It should be noted in this regard that there are SD calculations predicting the absence of light scalar excitations for $N_f > N_{fc}$ [18]. However, as already stressed no definitive conclusions can be drawn until finite size effects are under control.

Since our best chance of controlling the extrapolation to infinite volume appears to come from measurements of the order parameter, where signals are less noisy and finite volume effects relatively small, we now return to this and discuss results from $N_f = 2$ simulations at $\beta = 0.75$, closer to the continuum limit than our previous simulations. These datasets result from between 300 and 500 HMC trajectories. We studied the behaviour of the chiral condensate in detail in the large volume and small m_0 limits. Fig. 8 shows results for $\beta^2 \langle \bar{\Psi} \Psi \rangle$ vs. βm_0 extracted from simulations on system sizes $10^3, 20^3, 30^3, 40^3$ and 50^3 . These simulations were performed very close to the chiral limit ($m_0 \leq 0.005$). Although we don't extrapolate our data to the chiral limit it is clear that all the data tend to pass smoothly through the origin. A comparison of the 40^3 and 50^3 points shows that finite volume effects are under control, at least for $\beta m_0 \geq 0.0007$. Fig. 9 shows the same data zoomed to the vicinity of the origin. We can see that even when m_0 is very small, the data tend to pass smoothly through the origin: there is no indication of any tendency for the extrapolated intercept to be non-zero signalling chiral symmetry breaking. With the conservative criterion adopted above we conclude that for $N_f = 2$, $\beta^2 \langle \bar{\Psi} \Psi \rangle \leq 5 \times 10^{-5}$, which is a strong indication that chiral symmetry in QED₃ may be restored for $N_f \geq 2$.

In Figs. 8 and 9 we plotted the condensate vs. bare mass keeping the lattice volume L^3 constant along each line. Hitherto we have assumed that the physical volume of the system is proportional to $(L/\beta)^3$. If dynamical mass generation occurs by some means, however, so that a correlation length $\xi < \infty$ develops, then the correct measure of the physical volume is the ratio $(L/\xi)^3$ (this is merely the statement that finite volume effects are sensitive to which phase the theory resides in). This quantity varies along the constant lattice volume lines of Figs. 8,9 because ξ is in principle a function of both m_0 and β . We have attempted to study finite volume effects taking this possibility into account: since however we don't have an accurate estimate of a correlation length ξ either from the sigma mass, because of strong finite volume effects, or from the fermion mass, because the corresponding propagator is not gauge invariant, we are forced to estimate the behaviour of $\xi(\beta, m_0)$ directly from the condensate data. Since the precise relation between ξ and $\langle \bar{\Psi} \Psi \rangle$ is unknown, we proceed by observing that in all of our datasets for fixed β and $m_0 \geq 0.001$ it is approximately true that $\langle \bar{\Psi} \Psi \rangle \propto m_0$ and assuming that $\xi \propto \langle \bar{\Psi} \Psi \rangle^{-\alpha} \propto m_0^{-\alpha}$ for some power $\alpha = (d-1-\eta_{\bar{\Psi}\Psi})^{-1}$ where $\eta_{\bar{\Psi}\Psi}$ is the anomalous scaling dimension of the composite operator $\bar{\Psi}\Psi$. We then cover the range of possibilities by evaluating the condensate keeping Lm_0^α constant, with the choices $\alpha = \frac{1}{2}$ expected for a QCD-like theory in which $\eta_{\bar{\Psi}\Psi}$ is perturbatively small; and $\alpha = 1$, expected for a theory such as the NJL model in which $\eta_{\bar{\Psi}\Psi} \approx d-2$ and the condensate is directly proportional to the dynamically-generated scale. A value predicted for QED₃ with $N_f < N_{fc}$ by the SD approach is $\alpha = \frac{2}{3}$ corresponding to $\eta_{\bar{\Psi}\Psi} = \frac{1}{2}$ [5].

The results for $\beta = 0.75$ and $m_0 \geq 0$ are shown in Figs. 10 and 11 respectively. In the

case of the constant $L\sqrt{m_0}$ normalisation the lattice sizes for the three curves shown are $[50^3, 36^3, 30^3, 26^3, 22^3]$, $[40^3, 28^3, 24^3, 20^3, 18^3]$ and $[30^3, 22^3, 18^3, 16^3, 14^3]$. For constant Lm_0 the sequences are $[50^3, 26^3, 18^3, 14^3, 10^3]$, $[40^3, 20^3, 14^3, 10^3, 8^3]$ and $[30^3, 16^3, 10^3, 8^3, 6^3]$. By the very nature of the way the curves are produced an extrapolation to a non-trivial chiral limit is impossible, since eventually the assumption that $\langle\bar{\Psi}\Psi\rangle \propto m_0$ must break down; we note, however, that both sets of curves have negative curvature. It is also apparent that the curves with constant $L\sqrt{m_0}$ appear to approach the infinite volume limit uniformly over a wide range of m_0 , whereas those keeping Lm_0 constant diverge as m_0 increases. This is tentative evidence against a large value for $\eta_{\bar{\Psi}\Psi}$.

3.2 Deconfinement of Fractional Charge

Finally we consider a different issue, namely the confining properties of the theory. Since the gauge degrees of freedom are non-compact, matter fields and/or test charges may in principle be defined with any value of electric charge \tilde{g} which need not be commensurate with the dynamical fermion charge g . If the latter is the case, then such fractional charges should be confined by the Coulomb potential independent of the phase of the model, since long-range forces cannot in this case be screened by virtual $f\bar{f}$ pairs. It has been pointed out, however, that when the chiral symmetry of QED₃ is broken, either explicitly or spontaneously, then there may be a transition to a phase where fractional charge is deconfined at non-zero temperature [19].

In brief, on a system with finite extent T^{-1} in the Euclidean time direction, the action (2) has a global Z symmetry under non-periodic gauge transformations; in a static gauge this corresponds to invariance under

$$A_0(\vec{x}) \mapsto A_0(\vec{x}) + 2\pi\frac{nT}{g}, \quad n \in \mathbb{Z}. \quad (12)$$

It is readily seen that worldlines of all integer-charged matter fields are invariant under (12). For fractionally-charged particles, however, this is no longer the case. The analysis of [19] derives an effective potential $\mathcal{V}(A_0)$ which is periodic under (12); as T increases the barrier between non-equivalent minima of \mathcal{V} grows until the system becomes trapped near one such minimum, breaking the Z symmetry, with the fractionally-charged Polyakov line $\Pi_{\tilde{g}}(\vec{x}) = \exp i\tilde{g} \int_0^{T^{-1}} A_0(\vec{x}) dx_0$ acting as a gauge invariant order parameter. By analogy with Yang-Mills theory the symmetry broken phase is identified as one in which fractional charge is deconfined.

In the simulations of this paper we have not examined systems with the Euclidean time direction distinguished; however, we have found it interesting to check whether the Z symmetry is broken as a means of monitoring finite volume effects. We have chosen to examine charges which are rational fractions of the fundamental charge: $\tilde{g} = g/n$, and define the Polyakov loop $\Pi_n(\vec{x})$ by

$$\Pi_n(\vec{x}) = \prod_{t=1}^{L_t} \exp\left(\frac{i}{n}\theta_0(\vec{x}, t)\right). \quad (13)$$

The original Z symmetry (12) translates into a Z_n symmetry on Π_n ; spontaneous breaking is therefore signalled by a non-zero expectation of $\text{Re}(L^{-3} \sum_{\vec{x}} \Pi_n(\vec{x}))^n$. In Fig. 12 we plot

distributions of this quantity for $n = 1, 2, 4$ and 8 on a sequence of lattice volumes. On all systems the $n = 1$ data is sharply peaked about zero, indicating that there is no deconfinement of the fundamental integer charge¹. On 8^3 , however, the distributions for all $n \geq 2$ are skewed in the positive direction, indicating deconfinement. As the volume is increased, permitting fluctuations of the fields to develop over longer distances, the deconfinement signal is washed out until on 32^3 only charges with $\tilde{g} = g/8$ remain deconfined. A possible explanation of why smaller charges are harder to confine in a finite volume is that \tilde{g}^2 itself provides the scale in the logarithmic potential.

4 Summary and Outlook

In our study of QED₃ with $N_f \geq 2$ we attempted to establish whether chiral symmetry is broken or not by studying various observables close to the continuum limit $g \rightarrow 0$, on different volumes in order to detect and control finite size effects and near the chiral limit $m_0 \rightarrow 0$. As expected, susceptibilities and meson masses suffer from strong finite size effects and by themselves they do not allow us to reach a definitive conclusion. However, for the chiral condensate the continuum, thermodynamic and chiral limits are under better control. On the volumes we have been able to study we have seen no evidence for chiral symmetry breaking for any $N_f \geq 2$.

Our upper bound for the condensate in the $N_f = 2$ case is $\beta^2 \langle \bar{\Psi} \Psi \rangle \leq 5 \times 10^{-5}$, to be compared with the estimate for the quenched model $\beta^2 \langle \bar{\Psi} \Psi \rangle \approx 5 \times 10^{-3}$ [4, 12]. In addition, for all $N_f \geq 2$ the curves of $\beta^2 \langle \bar{\Psi} \Psi \rangle$ vs. βm_0 tend to pass smoothly through the origin with no sign of any discontinuous behaviour in N_f . This is evidence against the suggestion that the IR fixed point behaviour of QED₃ for $N_f \leq N_{fc}$ coincides with the UV behaviour of the three dimensional Thirring model as suggested by both the large- N_f expansion and SD studies [20]. For the Thirring model the critical N_{fc} below which a non-trivial UV fixed point exists has been estimated by Monte Carlo simulation to be $N_{fc} \simeq 5$ [20, 21]. The two models appear to lie in different universality classes, possibly because for $N_f < N_{fc}$ the Thirring model has no massless degree of freedom corresponding to the photon.

We are currently simulating the model with $N_f = 1$ to check whether in this case chiral symmetry is broken, as predicted by [11]. It will also be interesting in this respect to study whether the continuum $U(2N_f)$ symmetry is restored; this may entail the use of improved fermion actions [22] in future simulations. We also plan to extend our work to study in detail the deconfinement phase transition of fractional electric charges at $T > 0$.

¹More precisely, it suggests the free energy of an isolated fundamental charge diverges in the thermodynamic limit, which could also occur in the conformal phase.

Acknowledgements

SJH and CGS were supported by a Leverhulme Trust grant, and JBK in part by NSF grant PHY-0102409. The computer simulations were done on the Cray SV1's at NERSC, the IBM-SP at NPACI, and on the SGI Origin 2000 at the University of Wales Swansea. We have enjoyed discussions with Ian Aitchison, Nick Mavromatos, Sarben Sarkar and Rohana Wijewardhana.

References

- [1] N. Dorey and N.E. Mavromatos, Phys. Lett. **B250** (1990) 907; Nucl. Phys. **B386** (1992) 614;
K. Farakos and N.E. Mavromatos, Mod. Phys. Lett. **A13** (1998) 1019,
I.J.R. Aitchison, N. Dorey, M. Klein-Kreisler and N.E. Mavromatos, Phys. Lett. **B294** (1992) 91;
I.J.R. Aitchison, Z. Phys. **C67** (1995) 303.
- [2] B. Holdom, Phys. Lett. **B150** (1985) 301;
K. Yamawaki, M. Bando and K. Matumoto, Phys. Rev. Lett. **56** (1986) 1335;
T. Appelquist, D. Karabali and L.C.R. Wijewardhana, Phys. Rev. Lett. **57** (1986) 957.
- [3] R.D. Pisarski, Phys. Rev. **D29** (1984) 2423.
- [4] E. Dagotto, A. Kocić and J.B. Kogut, Nucl. Phys. **B334** (1990) 279.
- [5] T.W. Appelquist, M. Bowick, D. Karabali and L.C.R. Wijewardhana, Phys. Rev. **D33** (1986) 3704;
T.W. Appelquist, D. Nash and L.C.R. Wijewardhana, Phys. Rev. Lett. **60** (1988) 2575.
- [6] V.A. Miransky and K. Yamawaki, Phys. Rev. **D55** (1997) 5051;
V.P. Gusynin, V.A. Miranskii and A.V. Shpagin, Phys. Rev. **D58** (1998) 085023.
- [7] M.R. Pennington and S.R. Webb, Brookhaven preprint BNL-40886;
M.R. Pennington and D. Walsh, Phys. Lett. **B253** (1991) 246.
- [8] P. Maris, Phys. Rev. **D54** (1996) 4049.
- [9] D. Nash, Phys. Rev. Lett. **62** (1989) 3024;
K.-I. Kondo, T. Ebihara, T. Iizuka and E. Tanaka, Nucl. Phys. **B434** (1995) 85;
I.J.R. Aitchison, N.E. Mavromatos and D.O. McNeill, Phys. Lett. **B402** (1997) 154.
- [10] K.-I. Kubota and H. Terao, Prog. Theor. Phys. **105** (2001) 809.
- [11] T.W. Appelquist, A.G. Cohen and M. Schmaltz, Phys. Rev. **D60** (1999) 045003.
- [12] S.J. Hands and J.B. Kogut, Nucl. Phys. **B335** (1990) 455.

- [13] E. Dagotto, A. Kocić and J.B. Kogut, Phys. Rev. Lett. **62** (1989) 1083;
J.B. Kogut and J.-F. Lagaë, Nucl. Phys. **B**(Proc. Suppl.)**30** (1993) 737.
- [14] V. Azcoiti and X.-Q. Luo, Mod. Phys. Lett. **A8** (1993) 3635.
- [15] J. Alexandre, K. Farakos, S.J. Hands, G. Koutsoumbas and S.E. Morrison, Phys. Rev. **D64** (2001) 034502.
- [16] A.M. Polyakov, Nucl. Phys. **B120** (1977) 429;
T. Banks, R. Myerson and J.B. Kogut, Nucl. Phys. **B129** (1977) 493;
R.J. Wensley and J.D. Stack, Phys. Rev. Lett. **63** (1989) 1764;
M.N. Chernodub, E.M. Ilgenfritz and A. Schiller, Phys. Rev. Lett. **88** (2002) 231601.
- [17] C. Burden and A.N. Burkitt, Europhys. Lett. **3** (1987) 545.
- [18] T.W. Appelquist, J. Terning and L.C.R. Wijewardhana, Phys. Rev. Lett. **75** (1995) 2081.
- [19] G. Grignani, G. Semenoff and P. Sodano, Phys. Rev. **D53** (1996) 7157;
I.J.R. Aitchison and C.D. Fosco, Nucl. Phys. **B578** (2000) 199.
- [20] L. Del Debbio, S.J. Hands and J.C. Mehegan, Nucl. Phys. **B502** (1997) 269.
- [21] L. Del Debbio and S.J. Hands, Nucl. Phys. **B552** (1999) 339;
S.J. Hands and B. Lucini, Phys. Lett. **B461** (1999) 263.
- [22] C. Bernard *et al* (the MILC collaboration), Phys. Rev. **D58** (1998) 014503.

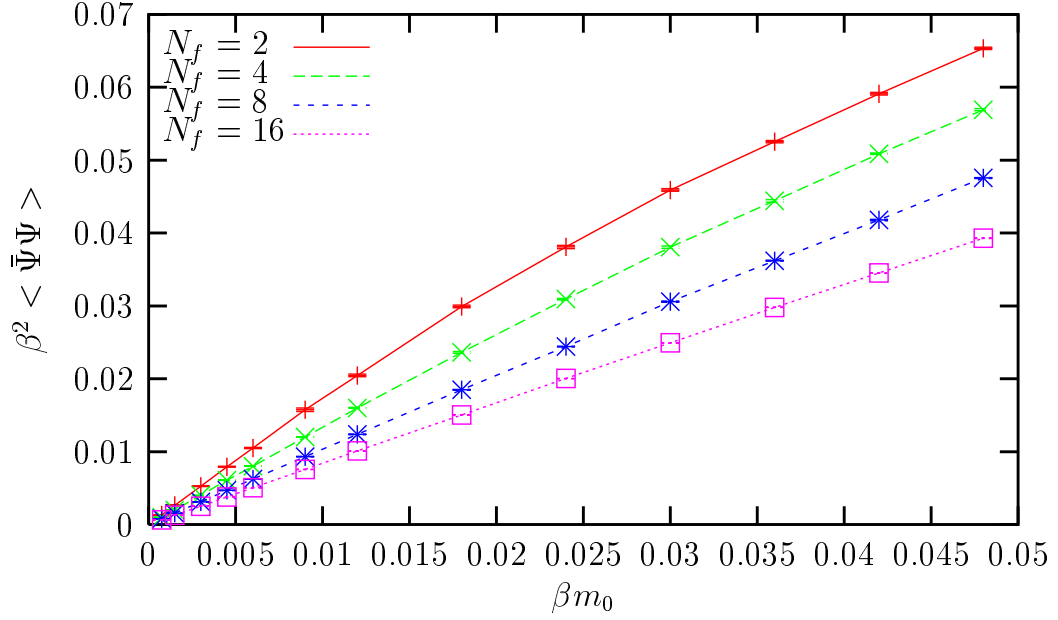


Figure 1: Dimensionless condensate $\beta^2 \langle \bar{\Psi} \Psi \rangle$ vs. dimensionless bare mass βm_0 for $N_f = 2, 4, 8, 16$, $\beta = 0.6$ on a 16^3 lattice.

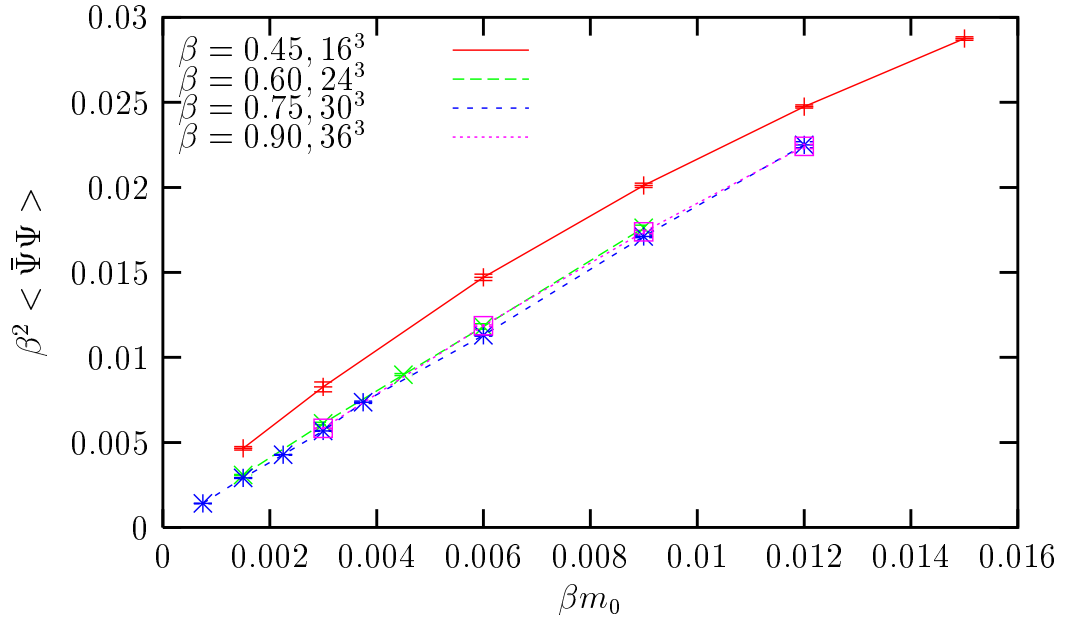


Figure 2: $\beta^2 \langle \bar{\Psi} \Psi \rangle$ vs. βm_0 for $N_f = 2$ at different values of the coupling β and constant physical volume $(L/\beta)^3$.

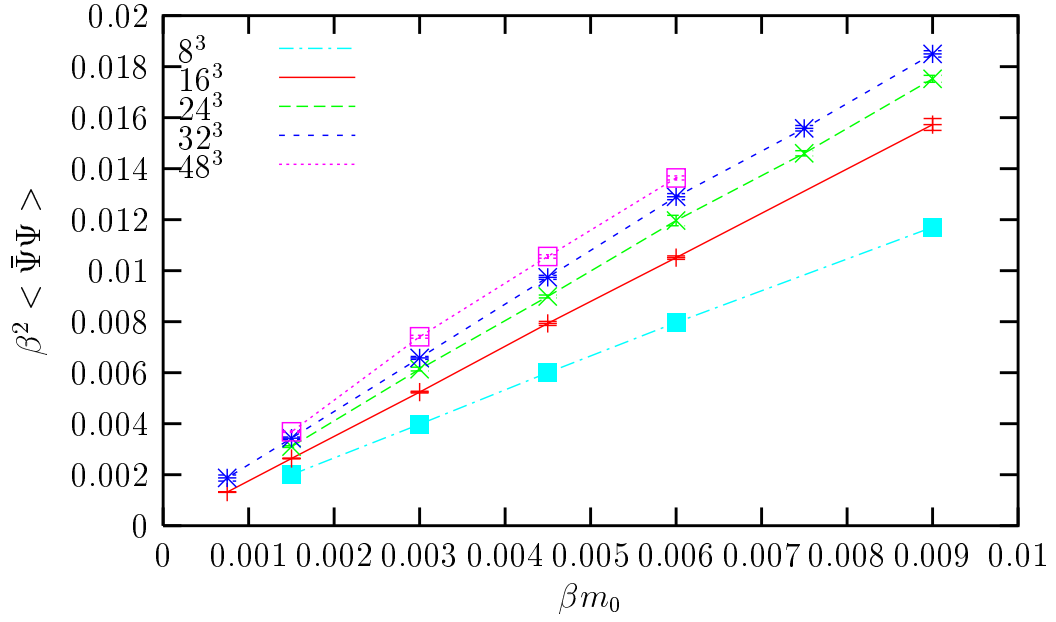


Figure 3: $\beta^2 \langle \bar{\Psi} \Psi \rangle$ vs. βm_0 for $N_f = 2$, $\beta = 0.6$ and lattice sizes $8^3, 16^3, 24^3, 32^3, 48^3$.

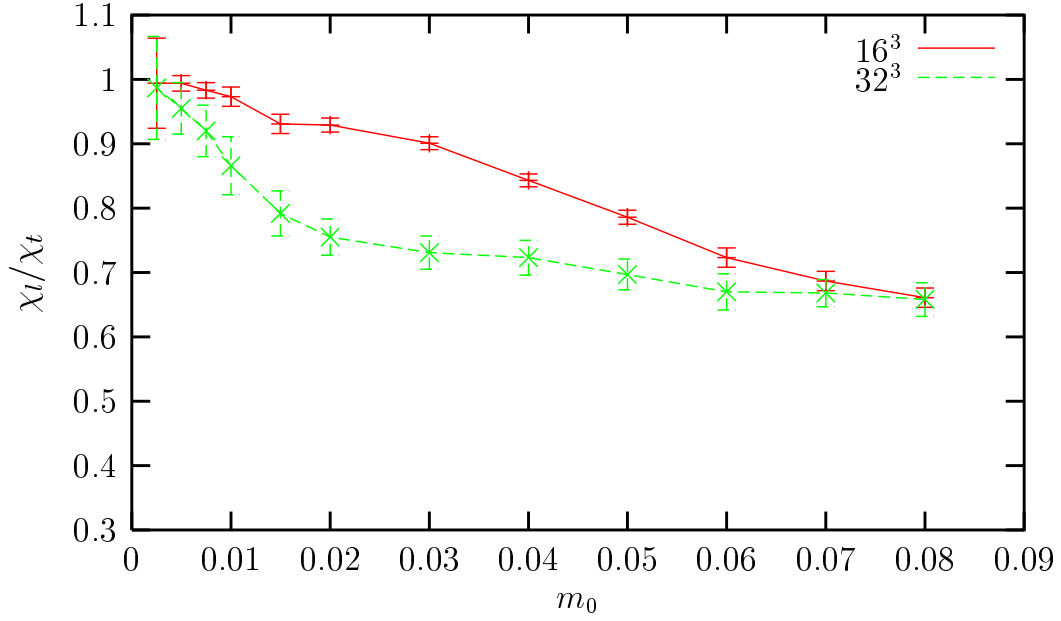


Figure 4: The ratio of longitudinal to transverse susceptibilities R vs. m_0 for $N_f = 2$, $\beta = 0.6$ on 16^3 and 32^3 lattices.

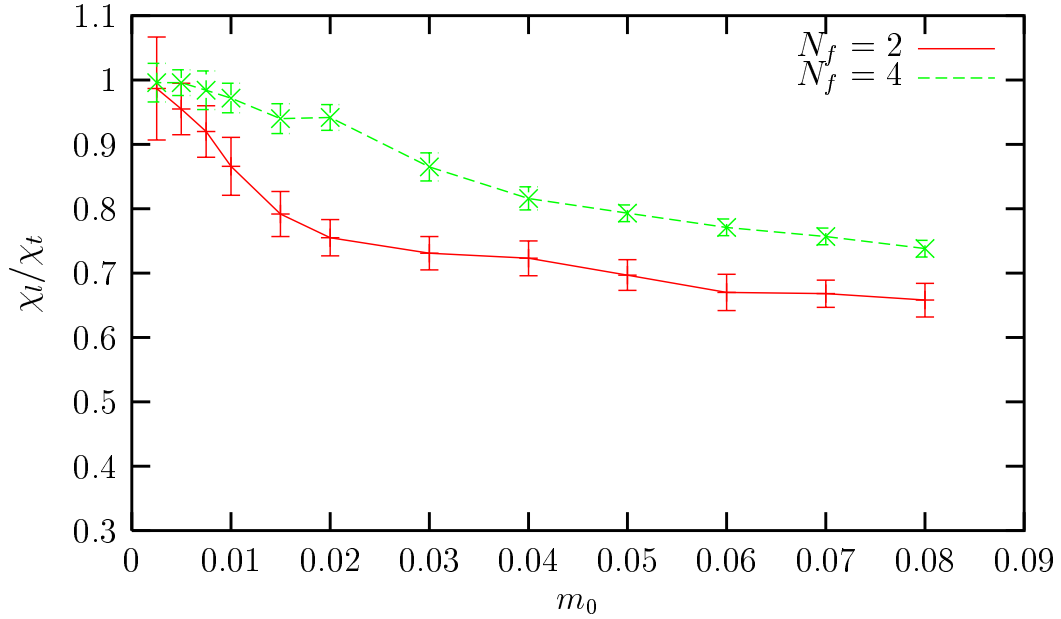


Figure 5: R vs. m_0 for $N_f = 2, 4$, $\beta = 0.6$ on 32^3 lattices.

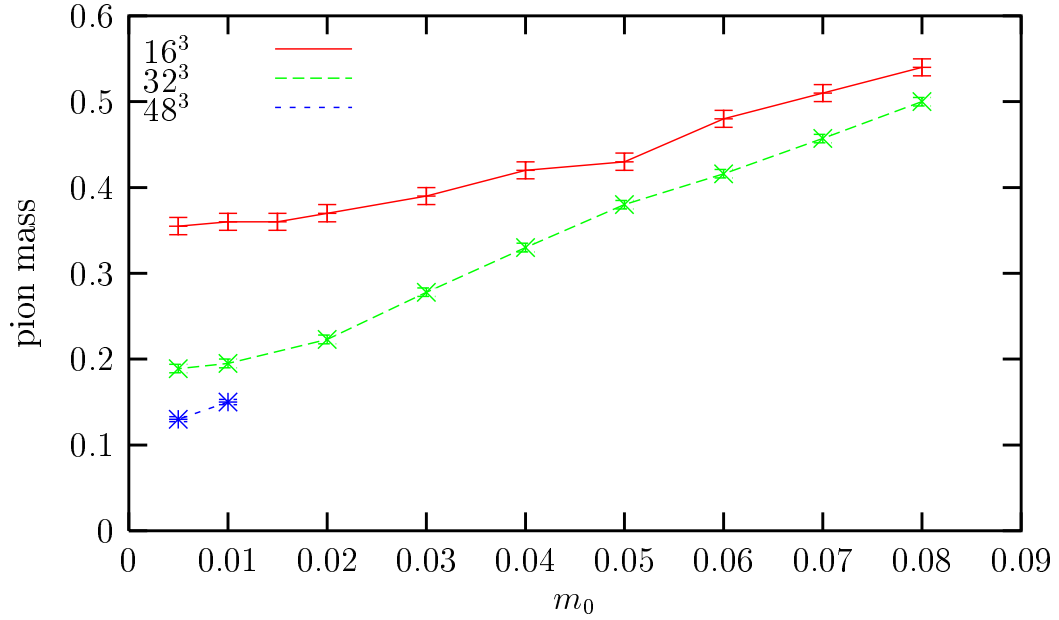


Figure 6: Pion mass vs. m_0 for $N_f = 2$, $\beta = 0.6$ on lattice sizes 16^3 , 32^3 and 48^3 .

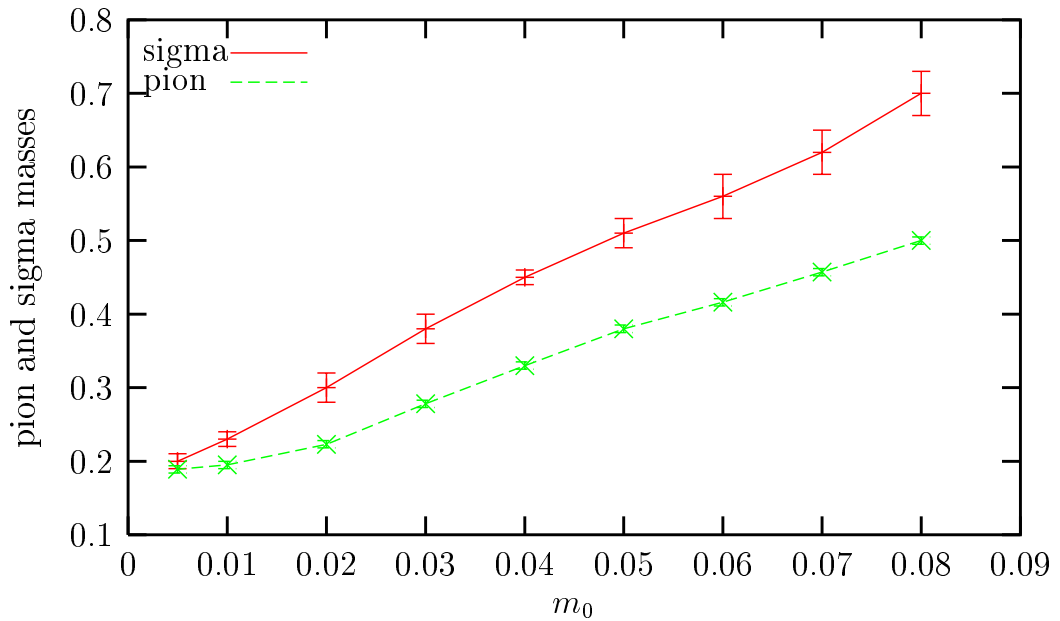


Figure 7: Masses of pion and sigma mesons vs. m_0 for $N_f = 2$, $\beta = 0.6$ on a 32^3 lattice.

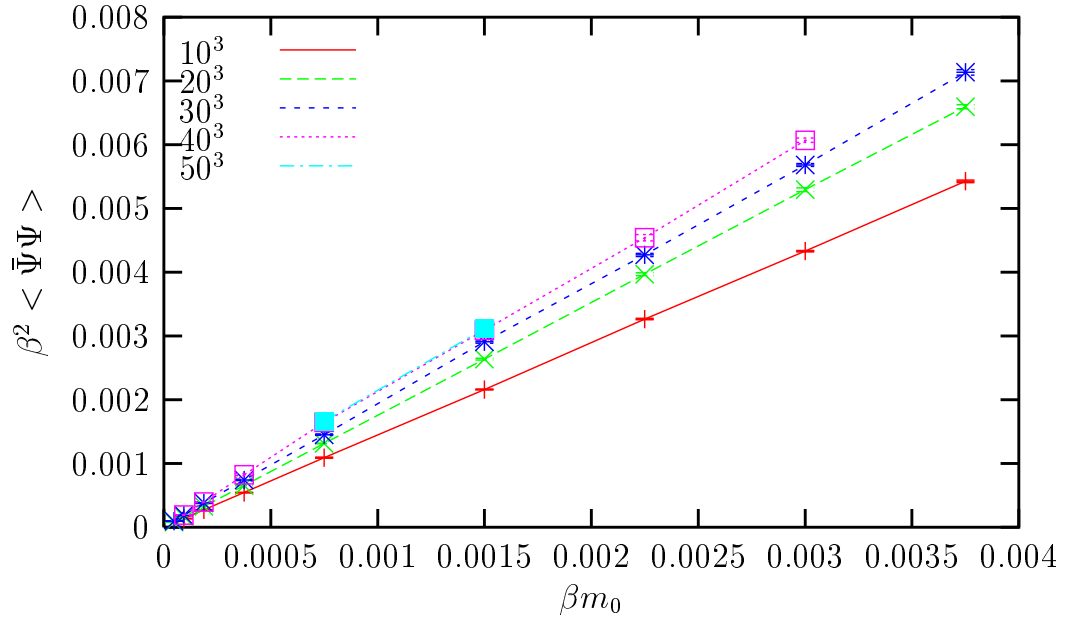


Figure 8: Condensate vs. bare mass for $N_f = 2$, $\beta = 0.75$ and lattice sizes $10^3, 20^3, 30^3, 40^3$ and 50^3 .

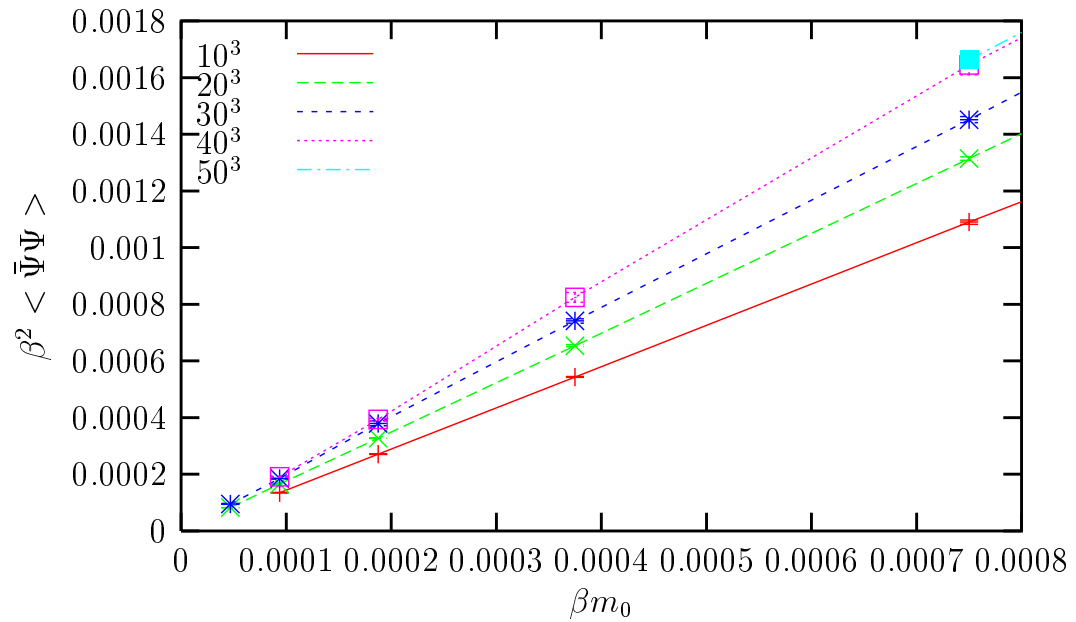


Figure 9: Same as Fig.8 but zoomed near the origin.

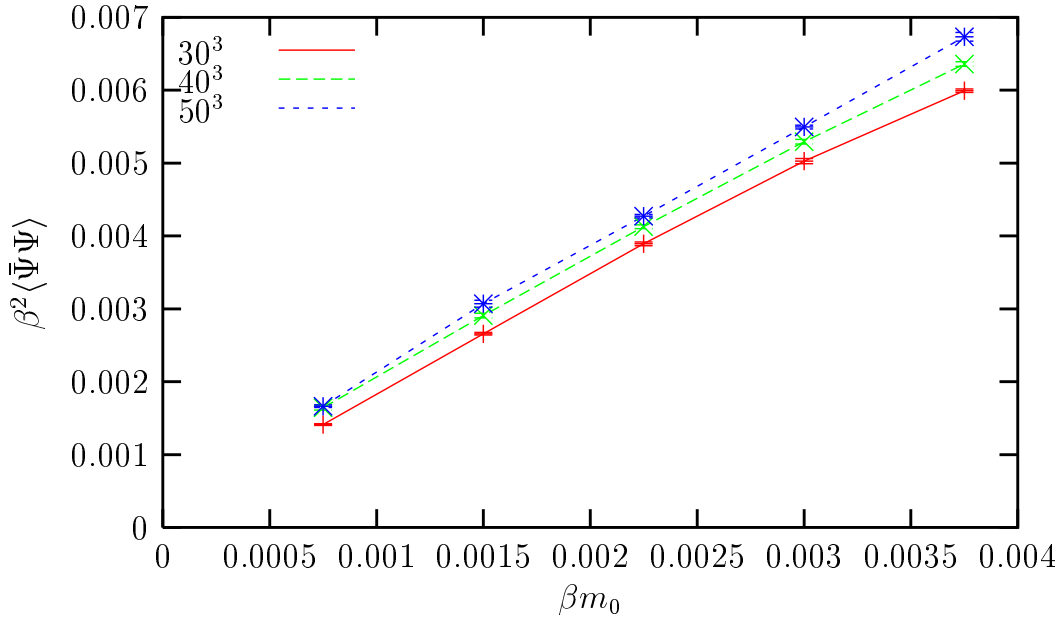


Figure 10: Condensate vs. fermion bare mass for $N_f = 2$ and $\beta = 0.75$ with $L\sqrt{m_0}$ kept approximately constant along each curve. The points at the smallest value of βm_0 were extracted from simulations on 50^3 , 40^3 and 30^3 lattices for each of the three different curves.

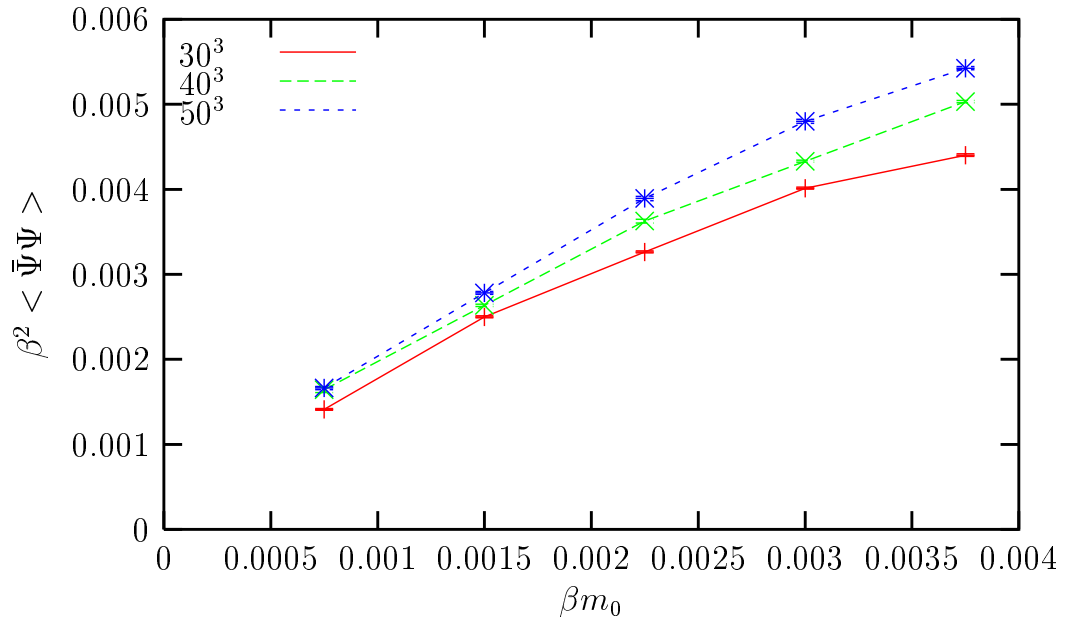


Figure 11: Condensate vs. fermion bare mass for $N_f = 2$ and $\beta = 0.75$ with Lm_0 kept approximately constant along each curve.

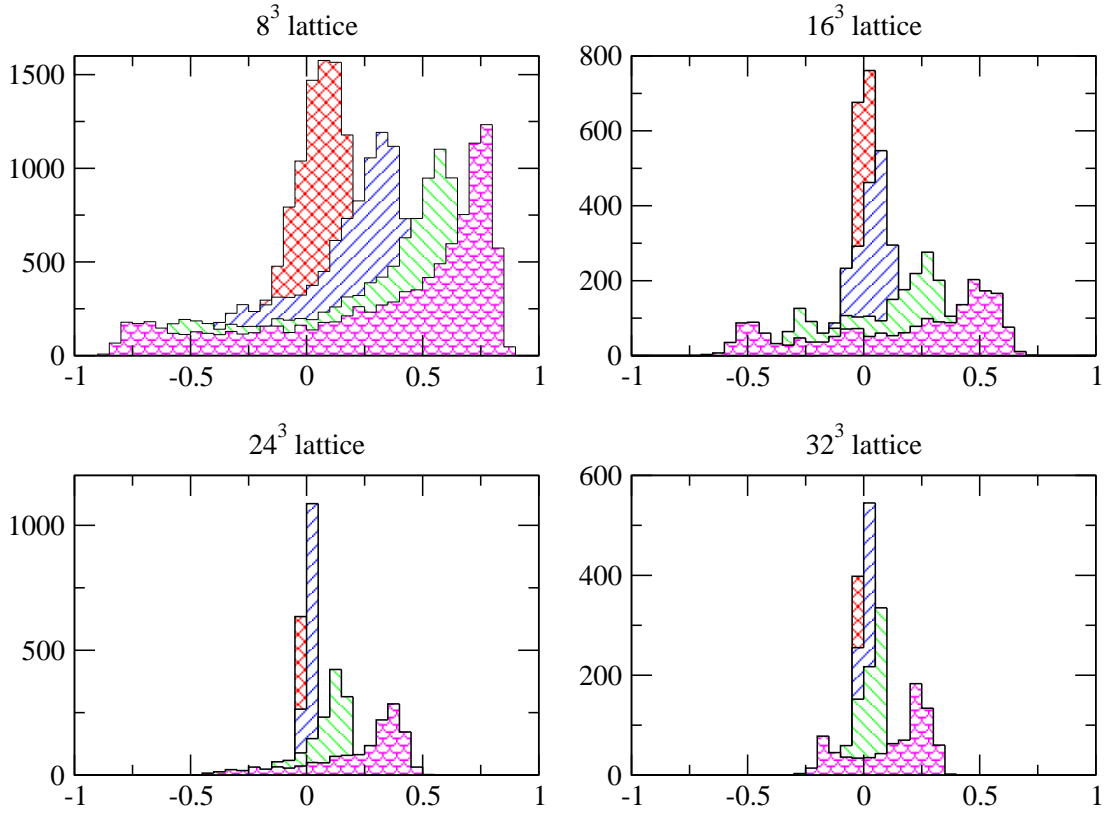


Figure 12: Histograms of the distribution of $\text{Re}(\Pi_n)^n$ from simulations with $N_f = 2$, $\beta = 0.6$ on 8^3 , 16^3 , 24^3 and 32^3 lattices, from respectively 10000, 2000, 1400 and 800 configurations. The squared shading denotes $n = 1$, cross-hatched to north-east $n = 2$, to north-west $n = 4$, and scalloped $n = 8$.